Heterogeneous Catalysis

International Edition: DOI: 10.1002/anie.201600463
German Edition: DOI: 10.1002/ange.201600463

Atomic-Scale Determination of Active Facets on the MoVTeNb Oxide M1 Phase and Their Intrinsic Catalytic Activity for Ethane Oxidative Dehydrogenation

Daniel Melzer, Pinghong Xu, Daniela Hartmann, Yuanyuan Zhu, Nigel D. Browning, Maricruz Sanchez-Sanchez,* and Johannes A. Lercher**

Abstract: *Aberration-corrected high-angle annular dark-field scanning transmission electron microscopy (HAADF-STEM) has been used to image the basal {001} plane of the catalytically relevant M1 phase in MoVTeNb complex oxides. Facets {010}, {120}, and {210} are identified as the most frequent lateral termination planes of the crystals. Combination of STEM with He ion microscopy (HIM) images, Rietveld analysis, and kinetic tests reveals that the activation of ethane is correlated to the availability of facets {001}, {120}, and {210} at the surface of M1 crystals. The lateral facets {120} and {210} expose crystalline positions related to the typical active centers described for propane oxidation. Conversely, the low activity of the facet {010} is attributed to its configuration, consisting of only stable M_6O_{21} units connected by a single octahedron. Thus, we quantitatively demonstrated that differences in catalytic activity among M1 samples of equal chemical composition depend primarily on the morphology of the particles, which determines the predominant terminating facets.*

Ethene and propene are important building blocks in the chemical industry. The availability of shale gas, as well as the interest in adding value to previously under-utilized carbon feedstocks, makes the production of ethene and propene by oxidative dehydrogenation (ODH) of the corresponding alkanes one of the most attractive alternatives to the current industrial practice of steam cracking.[1]

Among the existing catalysts, Mo-V-Te-Nb mixed oxides have shown high selectivity and activity in ODH of ethane to ethene,[2] propane to propene and selective (amm)oxidation to acrylic acid[3] and acrylonitrile.[3b,4] It is generally agreed that the crystalline phase M1 (Scheme 1) is responsible for the outstanding catalytic activity and selectivity of MoVTeNbOx, being the only phase able to catalyze the initial homolytic hydrogen abstraction from alkanes.[3a,5] Therefore, the crystallographic structure and composition of this phase has been extensively studied in the past decade.[6,7] M1 particles crystallize in shapes elongated in z direction,[8] but showing a broad range of morphologies ranging from particles with a flattened profile (Figure 1 A) to needle-like round rods (Figure 1 B) as shown by He ion microscopy (HIM). The ability of the M1 phase to activate alkanes has generally been ascribed to its basal [001] plane.[9] Celaya et al. suggested that not only the basal planes but also the lateral surface of M1 particles show activity in the reaction of propane to acrylic acid.[10] Later it was proposed that half-pipe hexagonal or heptagonal channels could expose active sites as well along the lateral of the particles.[11] However, apart from these studies, little attention has been devoted to the crystal termination of M1 and the nature of the lateral surface, even though, due to the elongated morphology of M1 particles, it can indeed account to up to more than 80% of the total surface.[9a]

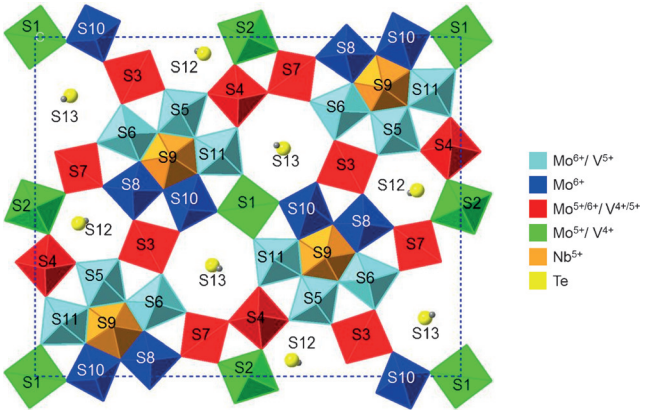

Scheme 1. Two-dimensional diagram of the MoVTeNbOx M1 unit cell viewed in the [001] direction with 13 cation sites labelled as in the literature.[6] Active site centers are composed by metal positions S2-S4-S7 (red and green), located between unit cells. Note that the polyhedra of different colors indicate compositions as labelled.

In this work, we explore quantitatively the relationship between morphology of M1 crystals and their activity in

[*] D. Melzer, D. Hartmann, Dr. M. Sanchez-Sanchez, Prof. Dr. J. A. Lercher
Department of Chemistry and Catalysis Research Center
Technische Universität München
Lichtenbergstraße 4, 85748 Garching (Germany)
E-mail: m.sanchez@tum.de
johannes.lercher@ch.tum.de
P. Xu
Department of Chemical Engineering and Materials Science
University of California, Davis
One Shields Avenue, Davis, CA 95616 (USA)
Dr. Y. Zhu, Prof. Dr. N. D. Browning
Fundamental and Computational Science Directorate
Pacific Northwest National Laboratory
Richland, WA 99352 (USA)
E-mail: nigel.browning@pnnl.gov

Supporting information for this article can be found under: http://dx.doi.org/10.1002/anie.201600463.

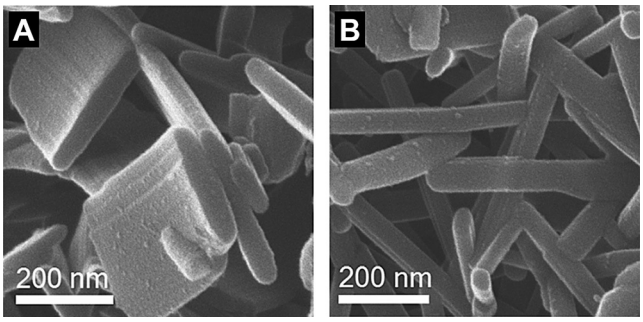

Figure 1. HIM images showing particles with the typical flattened particle morphology (A) and the typical rod-like morphology (B). Selected images from samples A and B in Table 1, respectively.

Table 1: Average morphology, facet frequency distribution, and activity in ethane ODH of three $MoVTeNbO_x$ catalysts showing different M1 phase morphologies.

Sample	A	B	C
morphology	flattened, large	rod-like	flattened, small
cross-section {001} [nm^2][a]	$3.9\times10^4\pm1.7\times10^4$	$1.4\times10^4\pm0.5\times10^4$	$1.5\times10^4\pm0.7\times10^4$
perimeter {001} [nm][a]	880 ± 230	530 ± 120	540 ± 120
length [nm][a]	500 ± 210	410 ± 130	430 ± 180
frequency of facet [%] [b]			
{010}	37 ± 8	28 ± 6	40 ± 7
{120}	31 ± 9	45 ± 7	21 ± 9
{210}	18 ± 5	16 ± 5	27 ± 5
{001}	15 ± 10	12 ± 7	12 ± 8
rate constant for ethane ODH at 643 K [$\mu mol\, g_{M1}^{-1}\, s^{-1}$]	145 ± 3	234 ± 4	187 ± 3

[a] Determined by HIM. Particle size distributions and statistical analysis in Section 5 of the Supporting Information. [b] Lateral facet distribution was determined by HAADF-STEM as shown in Figure 2 and the values were corrected to include contribution of the basal plane {001} with average particle size data obtained by HIM (details in Section 5 of the Supporting Information).

alkane activation. For this purpose, the oxidative dehydrogenation (ODH) of ethane was studied for a series of MoVTeNb mixed oxides showing different morphologies for the M1 crystalline phase. A detailed description of the materials and their catalytic activities is compiled in the Supporting Information. The reaction is known to follow first-order kinetics with respect to ethane.[12] The rate constants of all the studied samples were correlated with their M1 content as calculated by Rietveld analysis of the XRD patterns (see Figure S7-A in the Supporting Information). However, the rates normalized per M1 content did not provide a unified value within the error bar (Figure S7-B). Similar values of apparent energy of activation were obtained for the catalysts but the pre-exponential factors of the Arrhenius equation were very different, reflecting the divergences in normalized rates (see Figure S8). This indicates the existence of active sites with the same intrinsic activity in all samples, but a different concentration of available active sites per mass of M1 phase in each sample tested.

Since the ODH activity comparison is based on M1 samples with equal crystallinity and chemical composition, we hypothesize that the difference in the concentration of active sites is caused by the different morphologies of M1 particles. In order to probe this hypothesis, three MoVTeNbOx samples (labeled as A, B, and C in Table 1) containing particles with different morphology were examined by high-angle annular dark-field (HAADF) STEM images. As shown in Figure 2, the atomic resolution of STEM images allows identification of the facets that constitute the lateral termination of M1 particles. From this analysis, the length of each type of lateral facet was measured and the relative contribution of each facet to the total perimeter was quantified.

Analysis of more than ten randomly chosen M1 phase particles per sample demonstrates that the most frequently exposed lateral termination facets were {010}, {120}, and {210}. In order to calculate the fraction of surface area corresponding to each of the exposed crystalline phases, it is necessary to measure the average dimensions of M1 particles. Thus, over 50 particles were measured by HIM images for each sample. In this way, average values for perimeter and cross-section of {001} basal planes together with average particle lengths along the *z* axis were obtained (Table 1). The large error bars are due to the relatively broad size

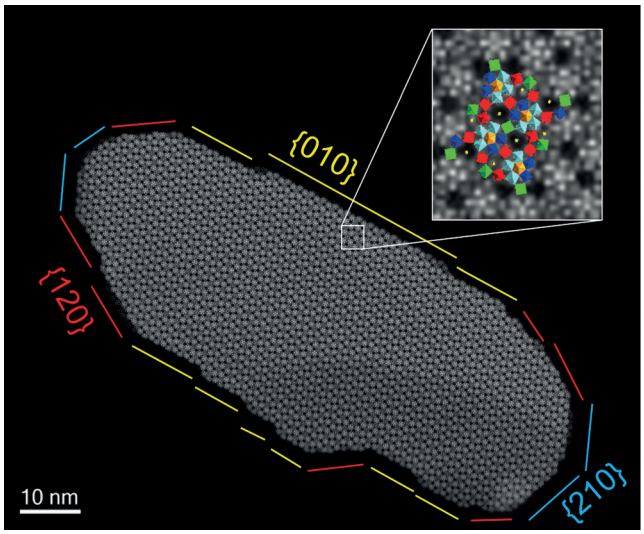

Figure 2. Unprocessed STEM image showing crystalline lateral termination facets of a typical flattened M1 particle viewed along [001] direction. In the inset, the scheme of a unit cell is overlapped with the image for guidance of the eye. Most frequent lateral surfaces {010}, {120}, and {210} have been marked. Symmetrically equivalent lateral surfaces have been marked with same color code.

distribution of M1 particles within a single sample. By using an estimated density of 1.14 $g\,cm^{-3}$ for M1, the total exposed surface area per gram of M1 phase was calculated for each of the most frequent surface facets (Table S1). Details of these calculations are given in the Supporting Information.

Once the exposed surface area of the different MoVTeNb samples has been described in terms of M1 crystal termination, the next step is to correlate the activity of the catalysts to

their surface structure. In Table 1, the rate constants of ethane ODH of samples A–C are shown normalized by mass of M1 phase (values for a temperature of 643 K). Figure 3 A shows these rate constants as a function of the surface area calculated for the different exposed facets in samples A–C. In Figure 3 A, it is expected to see an increase of activity with the increase of exposed surface area for those facets which are active, that is, exposing active sites. In that case, the slope represents the intrinsic activity for that particular facet, while the intercept is equivalent to the activity contribution of all the other facets. For the conventionally considered active plane {001}, it is evident that, although all three samples exhibit—within error bar—the same {001} surface area, the activity of the catalysts greatly deviates from each other (Figure 3, black circles). This strongly suggests that this facet alone cannot be responsible for the overall activity of the M1 particles. More interestingly, the lack of individual trends in Figure 3 A clearly shows that activity cannot be attributed solely to one facet.

In Figure 3 B, the ODH constant rate normalized per mass of M1 phase for the three samples A–C is plotted against

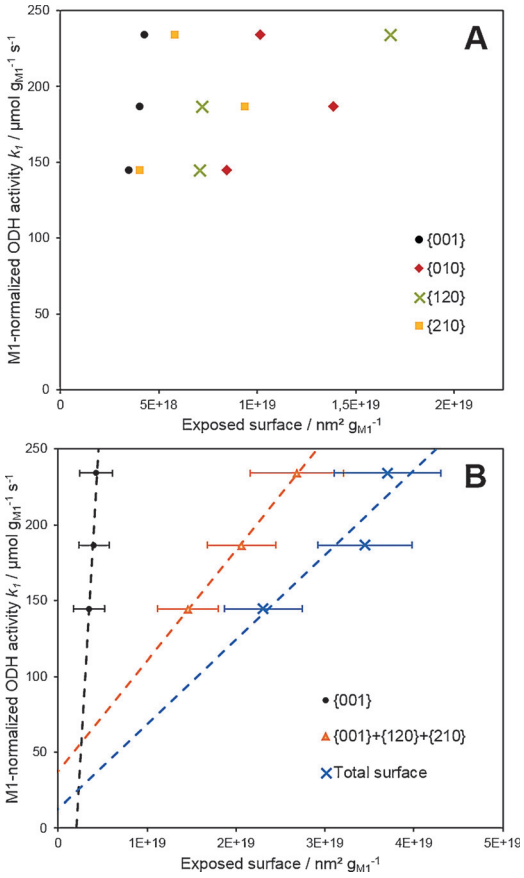

Figure 3. Catalytic activity of samples A to C normalized per content of M1 phase—as a function of the exposed surface areas calculated by statistical analysis of STEM and HIM images. A) Activity as a function of the surface area of individual frequent facets (error bars omitted for clarity, numeric values and uncertainties are given in Table S1 in Supporting Information), and B) comparison of activity for basal plane {001} with the combination of active facets and with the total surface area.

several combinations of surface facets exposed by their averaged particles (as calculated here from HIM and STEM statistical analysis). The error bars were calculated from the standard deviation of averaged values shown in Table 1 and the Gaussian error propagation laws. The good linear correlation obtained between the total exposed surface of M1 particles (approximated as the sum of the exposed surface area for {001}, {010}, {120}, and {210} facets) and the catalytic activity for ethane ODH, passing close to the origin, shows that multiple facets are involved in the reaction. Furthermore it proves the validity of the quantification of the overall exposed surface areas for each morphology type based in electron microscopy measurements. It must be noted that global magnitudes like BET area calculated by N_2 adsorption isotherms cannot be used in this case to normalize the activity of the catalysts because the presence of unavoidable small amounts of mesoporous amorphous material (with BET area ca. 100 $m^2 g^{-1}$ if textural properties of amorphous are similar to the synthetic precursor, Table S1) would yield misleadingly high surface areas.

In view of the above observations, the contribution of M1 facets other than {001} to ODH activity must be explored, requiring a detailed analysis of the termination of the lateral facets of M1 particles. Figure 4 illustrates the crystal termi-

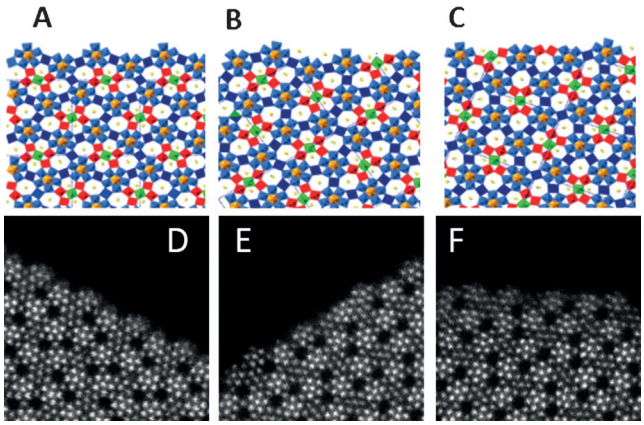

Figure 4. Rendering of the crystalline termination of the three most frequent facets viewed along [001] direction and according unprocessed STEM micrographs. Facet {010} is shown in (A) and (D), {120} in (B) and (E) and {210} in (C) and (F), respectively.

nation along the three most frequent lateral facets as found by atomic resolution STEM (Figure 2). As shown in Figure 4 A and Figure 4 D, {010} facets are purely composed of pentagonal M_6O_{21} units (metal positions S5, S6, S8, S9, S10 and S11 in Scheme 1) linked by single MO_6 octahedra (S3 in Scheme 1) following a smooth zigzag pattern. Neither the active center proposed by Grasselli et al.[9a] nor the half-pipe channels suggested by the research group of Schlögl[11b] are exposed in perfect {010} surfaces. Conversely, both the {210} and {120} facets consist of pentagonal units connected alternatively by single MO_6 octahedron or by a group of octahedra that make up half hexagonal or heptagonal rings.

Interestingly, the S2-S4-S7 metal positions in Scheme 1, proposed in the literature as the catalytic center for alkane

activation,[9a] are not exposed along the {010} facet. Conversely, the {120} and {210} facets would have S2-S4-S7 exposed at the half-pipe channels (hexagonal or heptagonal), as shown in Figure 4 B,E and C,F, respectively. Furthermore, we have observed that {010} facet tends to form the longest edges of the flattened particles, constituting this way the most abundant lateral facet (Table 1). We hypothesize that a densely packed configuration consisting of M_6O_{21} pentagonal units connected by single MO_6 octahedra represents the most stable termination of M1 crystal particles. Conversely, the existence of half heptagonal and hexagonal channels in the surface of the {120} and {210} facets constitute a more open structure and, thus, a lower stability termination, explaining why these facets are usually shorter than {010}. Hence, particles rich in {010} tend to be large and to present a flattened morphology, while particles rich in {210} and {120} facets present a small and rounded cross-section (i.e., {001} plane), as can be seen in Figure 1.

When the activity in ODH of MoVTeNbOx samples with different morphology is plotted against the combined surface area of those facets exposing active sites ({001} + {120} + {210}, Figure 3 B), a remarkably good linearity is obtained. Indeed, this correlation is better than the one obtained for the total surface of the particles (also in Figure 3 B) but with a small positive ordinate-axis intercept (ca. 35 $\mu mol\, g_{M1}^{-1} s^{-1}$). The only difference between these two correlations (total surface and active surface, Figure 3 B) is that the total surface includes the additional exposed surface area due to the presumably inactive {010} facet, which is hypothesized to be responsible for the deviation from linearity of this trend. Nevertheless, the *y* axis intercept and the different slope obtained for the sum of {001} + {120} + {210}, indicates that not all the surface sites were accounted by this approximation. We speculate that some activity is caused by small areas of higher index planes or dislocations such as steps or kinks in low index planes not accounted for in the present analysis. Indeed, it was possible to characterize by STEM images the existence of four types of steps in the intrinsically inactive {010}. As it can be seen in Figure 5, two of the nanosteps (type 1 and 4) are formed through a breakage across the S2-S4-S7 cluster and in that case open half-channel structures like in active facets {120} and {210} are exposed. The nanosteps for facets {120} and {210} have been also described (see Figures S3 and S4). It should be noted that the existence of active and inactive defects in intrinsically active facets does not affect the analysis performed in Figure 3 and conclusions thereafter.

Surface changes of MoVTeNb oxides when exposed to reaction conditions have been recently detected by different in situ techniques.[13] In consequence, models proposing some identifiable arrangement of M1 lattice sites as active centers, as discussed here, have been called into question. The present results show unequivocally and quantitatively that specific features in M1 phase MoVTeNb oxide are associated with the C–H activation. Whether these sites act as precursors and transform during catalysis or retain the structures discussed here is beyond the goal of the present contribution. However, the well-known stability of these catalysts and the reproducibility of their activity indicate that active sites are present in identical concentration and nature before and after exposure to reactant conditions. Thus, any surface dynamic transformation under reaction conditions must be reversible and, in that case, the role of M1 crystalline lattice can be envisioned as a structural precursor, providing the ground for the formation of the active sites.[13d] In that sense, morphology of the fresh M1 particles has been revealed to be crucial: particles with open and flexible lateral terminations render higher rates than those with densely packed lateral surfaces.

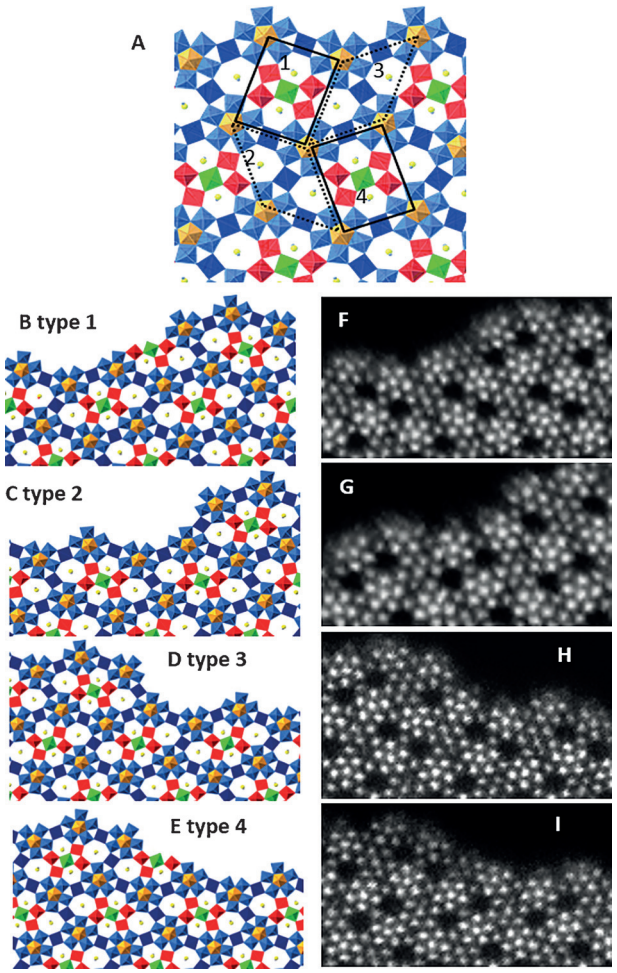

Figure 5. A) Rendering of termination mechanism of four different steps along {010} facets based on STEM images through breakage of bonding at 4 sites; B–E) Rending of the 4 nanoscale steps types formed through breakage of site 1–4, respectively. F–I) Unprocessed STEM images of nanoscale steps type 1–4, respectively. A similar analysis of the steps in facets {120} and {210} is available in the Supporting Information.

Combination of quantitative analysis of rates with statistical analysis by HIM and HAADF-STEM allowed linking the macroscopic catalytic rates to the atomic level description of active surfaces, which constitutes a first basis for understanding selective oxidation catalysis on atomistic level. The elucidation of the relationship between catalytic activity and crystal morphology for complex mixed oxide catalysts provides new tools for the design and optimization of synthetic methods directed to more active and selective catalysts.

Experimental Section

MoVTeNbOx catalysts were prepared by hydrothermal synthesis (details are given in the Supporting Information). Catalytic tests in ethane oxidative dehydrogenation were performed in the temperature range 603–703 K at conversions from 5 to 40 %. At the reaction conditions applied, high ethene selectivities (≥ 93 %) were obtained for all the samples. Further details are given in the supporting material. The morphology of M1 phases was characterized by a Zeiss Orion Helium Ion Microscope in the Environmental Molecular Sciences Laboratory (EMSL) at the Pacific Northwest National Laboratory (PNNL) with operating voltage at 30 keV and beam current < 1.0 pA. The sample was mounted onto the stub by commonly used carbon tape with a minimum carbon coating applied to sample that is < 5 nm. HR-STEM imaging was accomplished on an FEI aberration-corrected Titan 80/300 TEM/STEM operated at 300 kV and housed in EMSL at PNNL. All HAADF-STEM images in this report were acquired with a convergence semiangle of 17 mrad after fine tuning of the probe corrector. ADF detector semiangles of about 75–200 mrad were used. The spatial resolution achieved on a standard gold sample (Ted-Pella) was approximately 1 Å prior to STEM imaging of the samples. Samples for facet identification and quantification were prepared through microtome technique. Further details of the methods are provided in the Supporting Information.

Acknowledgements

This work was supported by the United States Department of Energy (DOE) grant number DE-FG02-03ER46057 through the University of California at Davis, the Laboratory Directed Research and Development (LDRD) Program: Chemical Imaging Initiative at Pacific Northwest National Laboratory (PNNL), and the Environmental Molecular Sciences Laboratory (EMSL), a national scientific user facility sponsored by the DOE's Office of Biological and Environmental Research and located at PNNL. PNNL is a multiprogram national laboratory operated by Battelle for the DOE under grant number DE-AC05-76RL01830.

Keywords: heterogeneous catalysis · oxidative dehydrogenation · scanning probe microscopy · surface chemistry · surface structures

How to cite: *Angew. Chem. Int. Ed.* **2016**, *55*, 8873–8877
Angew. Chem. **2016**, *128*, 9019–9023

[1] F. Cavani, N. Ballarini, A. Cericola, *Catal. Today* **2007**, *127*, 113–131.

[2] a) C. A. Gärtner, A. C. van Veen, J. A. Lercher, *ChemCatChem* **2013**, *5*, 3196–3217; b) T. T. Nguyen, M. Aouine, J. M. M. Millet, *Catal. Commun.* **2012**, *21*, 22–26; c) J. M. L. Nieto, P. Botella, M. I. Vazquez, A. Dejoz, *Chem. Commun.* **2002**, 1906–1907; d) T. T. Nguyen, B. Deniau, P. Delichere, J.-M. M. Millet, *Top. Catal.* **2014**, *57*, 1152–1162; e) P. Botella, E. García-González, A. Dejoz, J. M. López Nieto, M. I. Vázquez, J. M. González-Calbet, *J. Catal.* **2004**, *225*, 428–438.

[3] a) D. Vitry, Y. Morikawa, J. L. Dubois, W. Ueda, *Top. Catal.* **2003**, *23*, 47–53; b) W. A. Goddard, L. Liu, J. E. Mueller, S. Pudar, R. J. Nielsen, *Top. Catal.* **2011**, *54*, 659–668; c) J. M. Oliver, J. M. L. Nieto, P. Botella, *Catal. Today* **2004**, *96*, 241–249; d) P. Concepción, S. Hernández, J. M. L. Nieto, *Appl. Catal. A* **2011**, *391*, 92–101.

[4] K. Muthukumar, J. Yu, Y. Xu, V. V. Guliants, *Top. Catal.* **2011**, *54*, 605–613.

[5] P. Botella, E. García-González, J. M. López Nieto, J. M. González-Calbet, *Solid State Sci.* **2005**, *7*, 507–519.

[6] P. DeSanto, J. Buttrey Douglas, K. Grasselli Robert, G. Lugmair Claus, F. Volpe Anthony, H. Toby Brian, T. Vogt, *Z. Kristallogr.* **2004**, *219*, 152.

[7] a) W. D. Pyrz, D. A. Blom, T. Vogt, D. J. Buttrey, *Angew. Chem. Int. Ed.* **2008**, *47*, 2788–2791; *Angew. Chem.* **2008**, *120*, 2830–2833; b) D. A. Blom, X. Li, S. Mitra, T. Vogt, D. J. Buttrey, *ChemCatChem* **2011**, *3*, 1028–1033; c) W. D. Pyrz, D. A. Blom, N. R. Shiju, V. V. Guliants, T. Vogt, D. J. Buttrey, *J. Phys. Chem. C* **2008**, *112*, 10043–10049; d) X. Li, D. J. Buttrey, D. A. Blom, T. Vogt, *Top. Catal.* **2011**, *54*, 614–626.

[8] P. DeSanto, D. J. Buttrey, R. K. Grasselli, C. G. Lugmair, A. F. Volpe, B. H. Toby, T. Vogt, *Top. Catal.* **2003**, *23*, 23–38.

[9] a) R. K. Grasselli, D. J. Buttrey, P. DeSanto, J. D. Burrington, C. G. Lugmair, A. F. Volpe, T. Weingand, *Catal. Today* **2004**, *91–92*, 251–258; b) N. R. Shiju, X. Liang, A. W. Weimer, C. Liang, S. Dai, V. V. Guliants, *J. Am. Chem. Soc.* **2008**, *130*, 5850–5851; c) S. Ishikawa, D. Kobayashi, T. Konya, S. Ohmura, T. Murayama, N. Yasuda, M. Sadakane, W. Ueda, *J. Phys. Chem. C* **2015**, *119*, 7195–7206.

[10] A. Celaya Sanfiz, T. W. Hansen, A. Sakthivel, A. Trunschke, R. Schlögl, A. Knoester, H. H. Brongersma, M. H. Looi, S. B. A. Hamid, *J. Catal.* **2008**, *258*, 35–43.

[11] a) W. Zhang, A. Trunschke, R. Schlögl, D. Su, *Angew. Chem. Int. Ed.* **2010**, *49*, 6084–6089; *Angew. Chem.* **2010**, *122*, 6220–6225; b) R. Schlögl, *Top. Catal.* **2011**, *54*, 627–638.

[12] J. B. Wagner, O. Timpe, F. A. Hamid, A. Trunschke, U. Wild, D. S. Su, R. K. Widi, S. B. A. Hamid, R. Schlögl, *Top. Catal.* **2006**, *38*, 51–58.

[13] a) M. Hävecker, S. Wrabetz, J. Kröhnert, L.-I. Csepei, R. Naumann O'Alnoncourt, Y. V. Kolen'ko, F. Girgsdies, R. Schlögl, A. Trunschke, *J. Catal.* **2012**, *285*, 48–60; b) C. Heine, M. Hävecker, M. Sanchez-Sanchez, A. Trunschke, R. Schlögl, M. Eichelbaum, *J. Phys. Chem. C* **2013**, *117*, 26988–26997; c) C. Heine, M. Havecker, A. Trunschke, R. Schlögl, M. Eichelbaum, *Phys. Chem. Chem. Phys.* **2015**, *17*, 8983–8993; d) D. A. Blom, T. Vogt, L. F. Allard, D. J. Buttrey, *Top. Catal.* **2014**, *57*, 1138–1144.

Received: January 15, 2016
Published online: March 16, 2016

